Journal of Biomechanics 42 (2009) 234–241

Contents lists available at ScienceDirect

Journal of Biomechanics

journal homepage: www.elsevier.com/locate/jbiomech
www.JBiomech.com

Validation of subject-specific automated p-FE analysis of the proximal femur

Nir Trabelsi [a], Zohar Yosibash [a,*], Charles Milgrom [b]

[a] Department of Mechanical Engineering, Ben-Gurion University, Beer-Sheva 84105, Israel
[b] Department of Orthopaedics, Hadassah University Hospital, Jerusalem, Israel

ARTICLE INFO

Article history:
Accepted 28 October 2008

Keywords:
Proximal femur
Finite element analysis
p-FEM
Computed tomography (CT)
Bone biomechanics

ABSTRACT

Background: The use of subject-specific finite element (FE) models in clinical practice requires a high level of automation and validation. In Yosibash et al. [2007a. Reliable simulations of the human proximal femur by high-order finite element analysis validated by experimental observations. J. Biomechanics 40, 3688–3699] a novel method for generating high-order finite element (p-FE) models from CT scans was presented and validated by experimental observations on two fresh frozen femurs (harvested from a 30 year old male and 21 year old female). Herein, we substantiate the validation process by enlarging the experimental database (54 year old female femur), improving the method and examine its robustness under different CT scan conditions.

Approach: A fresh frozen femur of a 54 year old female was scanned under two different environments: in air and immersed in water (dry and wet CT). Thereafter, the proximal femur was quasi-statically loaded in vitro by a 1000 N load. The two QCT scans were manipulated to generate p-FE models that mimic the experimental conditions. We compared p-FE displacements and strains of the wet CT model to the dry CT model and to the experimental results. In addition, the material assignment strategy was reinvestigated. The inhomogeneous Young's modulus was represented in the FE model using two different methods, directly extracted from the CT data and using continuous spatial functions as in Yosibash et al. [2007a. Reliable simulations of the human proximal femur by high-order finite element analysis validated by experimental observations. J. Biomechanics 40, 3688–3699].

Results: Excellent agreement between dry and wet FE models was found for both displacements and strains, i.e. the method is insensitive to CT conditions and may be used in vivo. Good agreement was also found between FE results and experimental observations. The spatial functions representing Young's modulus are local and do not influence strains and displacements prediction. Finally, the p-FE results of all three fresh frozen human femurs compare very well to experimental observations exemplifying that the presented method may be in a mature stage to be used in clinical computer-aided decision making.

1. Introduction

Accurate methods for predicting and monitoring in vivo bone strength are of major importance in clinical applications. Subject-specific finite element (FE) modeling is becoming a commonly used tool for the numerical analysis of the biomechanical response of human bones. The use of subject-specific FE models in clinical practice requires a high level of automation and an accurate evaluation of the numerical errors. Geometry and material parameters are two key components when addressing subject-specific FE models of bones and both can be estimated from quantitative CT (QCT) data. Generation of a FE model requires extensive processing of QCT data. Because CT-based simulations are to be used in vivo, the surrounding of the bone may influence the model generation and the influence on the results must be carefully examined. For example, Keyak and Falkinstein (2003) examined whether FE models generated from CT scans in situ and in vitro yield comparable predictions of proximal femoral fracture load. Their conclusion is that substantially different predicted fracture loads are noticed.

The influence of material assignment strategy to FE models was investigated e.g. in Helgason et al. (2008); Schileo et al. (2007); Taddei et al. (2007); Peng et al. (2006). In Taddei et al. (2007) two methods were compared to experimental measurements, the first used a classical strategy of calculating Young's modulus from an average element density, the second calculated the average of Young's modulus that was directly derived from each CT slice. The results showed that the two strategies produced two distributions of material properties that were statistically different. Strain predictions showed that the second method is in a better agreement with the experimental results. In Helgason et al. (2008) a comparison was made between two different methods for assigning material properties to FE models. A modified material assignment strategy allowing for spatial variation of Young's modulus within the elements was presented and compared to a more conventional strategy, whereby constant

* Corresponding author. Tel.: +972 8 6477103.
E-mail address: zohary@bgu.ac.il (Z. Yosibash).

0021-9290/$ - see front matter © 2008 Elsevier Ltd. All rights reserved.
doi:10.1016/j.jbiomech.2008.10.039

Fig. 1. Bone and K_2HPO_4 phantoms scans under two different conditions wet CT (left) and dry CT (right).

material properties are assigned to each element. The first method performs better when strain prediction is of interest. Limited number of studies have been dedicated to systematic validation of subject-specific FE models of femoral bones by comparison to experiments. A good accuracy ($R^2 > 0.8$) in the prediction of strain levels was reported in recent works by Helgason et al. (2008) and Bessho et al. (2007) (displacements were not reported). Conventional h-version FE methods (h-FEM) were used in most FE studies (see e.g. Keyak et al., 1990; Cody et al., 1999; Schileo et al., 2007) with inhomogeneous distribution of material properties obtained by assigning constant distinct values to different elements—this caused the material properties to become mesh dependent (Taddei et al., 2007). Furthermore, same relation between Young's modulus and bone density $E(\rho)$ is considered both in the trabecular and cortical subregions although many studies report on different relations in the cortical and trabecular regions (Carter and Hayes, 1977; Cody et al., 2000; Wirtz et al., 2000).

In Yosibash et al. (2007a) a p-FE method was suggested, and an inhomogeneous Young's modulus was represented by smooth functions, independent of the mesh, having different $E(\rho)$ relations in the cortical and trabecular subregions. Herein, we further validate and improve the method presented in Yosibash et al. (2007a) and examine it under different CT scan conditions. The material assignment strategy is reinvestigated to evaluate the numerical errors inherent in it. In Yosibash et al. (2007a) two experiments on fresh frozen human femurs (30 year old male and 21 year old female) were conducted and observations were used for the validation of the FE model. Herein, a fresh frozen femur of a 54 year old female is scanned by two separate QCT scans. In the first (wet CT) the bone was immersed in water to simulate in vivo condition and to reduce beam hardening effects. In the second scan (dry CT) the bone was exposed to air. Thereafter the proximal femur was loaded (in vitro experiments) by a quasi-static force of 1000 N. The data from the two QCT scans were used to determine the geometrical representation of the femur and determination of its material properties, followed by generation of p-FE models. These were subjected to boundary conditions so to mimic the experiment conditions. We compared displacements and strains computed using the wet CT model with the ones obtained from the dry CT model. Young's modulus representation strategy was reinvestigated by two different methods, directly extracted from the CT data using weighted point average (WPA) and by several continuous spatial functions describing the inhomogeneous bone density with monotonic increase in polynomial degree. Experimental observations were used to validate FE results.

2. Methods

A fresh frozen femur of a 54 year old female donor was deep-frozen shortly after death. The bone was checked to be free of skeletal diseases as described in Yosibash et al. (2007a). After defrosting, soft tissue was removed from the bone and was degreased with ethanol. The proximal femur was cut and fixed concentric into a cylindrical sleeve by six bolts and a PMMA substrate and scanned in two different environments. QCT scans were performed using a Phillips Brilliance 16 CT (Eindhoven, Netherlands) with the following parameters: 120 kVp, 250 mAs, 1.25 mm slice thickness, axial scan without overlap, and pixel size of 0.5176 mm (512 pixels covering 265 mm field size). In the wet scan (CTwet) the bone was immersed in water. Five burettes (calibration phantoms) containing different concentrations of K_2HPO_4 ranging from 0 to 300 mg/cm^3 were placed in the tub close to the bone (see Fig. 1 left). The aim of this scan was to simulate in situ conditions and reduce beam hardening effects (Luo, 2003). Following the QCT stain-gauges (SGs) were bonded using M-Bond 200 cyanoacrylate adhesive. A second scan (CTdry) was performed to the bone exposed to air (Fig. 1 right). This enables to identify the exact location of the SGs. Mechanical experiments started 8 h after bone mounting, long enough for the PMMA to cure, and lasted for 20 h (bone was constantly hydrated). Two p-FE models were generated based on QCT scans. The geometric representation, material properties evaluation and analysis results were compared. p-FE simulations that mimic the experiments were performed and results were compared to experimental observations.

2.1. In vitro experiment

The experimental system is described in Yosibash et al. (2007a). Bone was loaded by a load controlled machine (Instron 5500R). Two linear variable differential transformer (LVDT) measured the femur head vertical and horizontal displacements (core placed on femur's head), see Fig. 2. Eleven uni-axial SGs (Vishay CEA-06-062UR-350) with 1.6 mm active length and 350 Ω resistance were installed on the proximal femur at the inferior and superior parts of the femur neck and on the medial and lateral femur shaft. SGs, load–cell and the LVDT outputs were recorded (except of four SGs that failed due to bonding problems). The experiments simulate a simple stance position configuration in which the femur is loaded through its head while it is inclined at four different angles (0°, 7°, 15° and 20°), see Fig. 2.

2.2. p-FE models

Geometry creation and assignment of material properties to the FE mesh are detailed in Yosibash et al. (2007a). The method in Yosibash et al. (2007a) was applied to both CTwet and CTdry data, generating two independent FE models. All DICoM format QCT scans were automatically manipulated by MatLab[1] based programs. Averaged *HU*'s were converted to an equivalent mineral density ρ_{EQM} [g/cm^3]. The linear relation ρ_{EQM} (*HU*) was determined by calibration phantoms (see Fig. 3). Femur's geometry was extracted from QCT slices and divided into three main subregions (see Fig. 4): the cortical subregion ($\rho_{EQM} > 0.45, 0 < z < 113.75$ mm), the trabecular subregion ($\rho_{EQM} < 0.45, 62.25 < z < 113.75$ mm) and the head-trochanter subregion ($113.5 < z < 155$ mm). Exterior, interface and interior boundaries were traced at each slice. A smoothing algorithm was applied that generate smooth closed splines used for the solid body creation. The solid body was meshed by an auto-mesher with tetrahedral elements using p-FE StressCheck[2] code. Blending function method maps the elements to the standard element so the surfaces are accurately represented. Young's modulus $E(x, y, z)$ was determined from *HU* arrays obtained from CT slices. A moving average algorithm was applied with a pre-defined cubic volume of 3×3 mm^3 (see Yosibash et al., 2007b). *HU* averaged values were converted to an equivalent mineral density ρ_{EQM} according to calibration phantoms (Eqs. (1) and (2)). Two methods for representing

[1] MatLab is trademark of The MathWorks Inc., MA, USA.

[2] StressCheck is trademark of Engineering Software Research and Development, Inc., St. Louis, MO, USA.

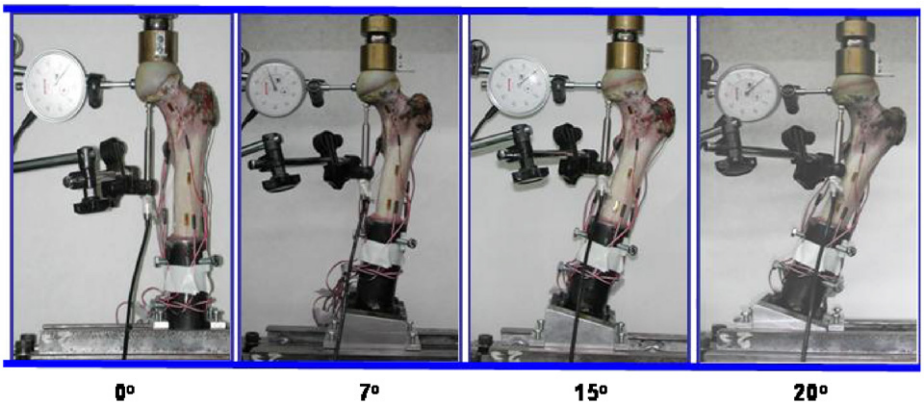

Fig. 2. Experiments on the fresh frozen bone at different inclination angles.

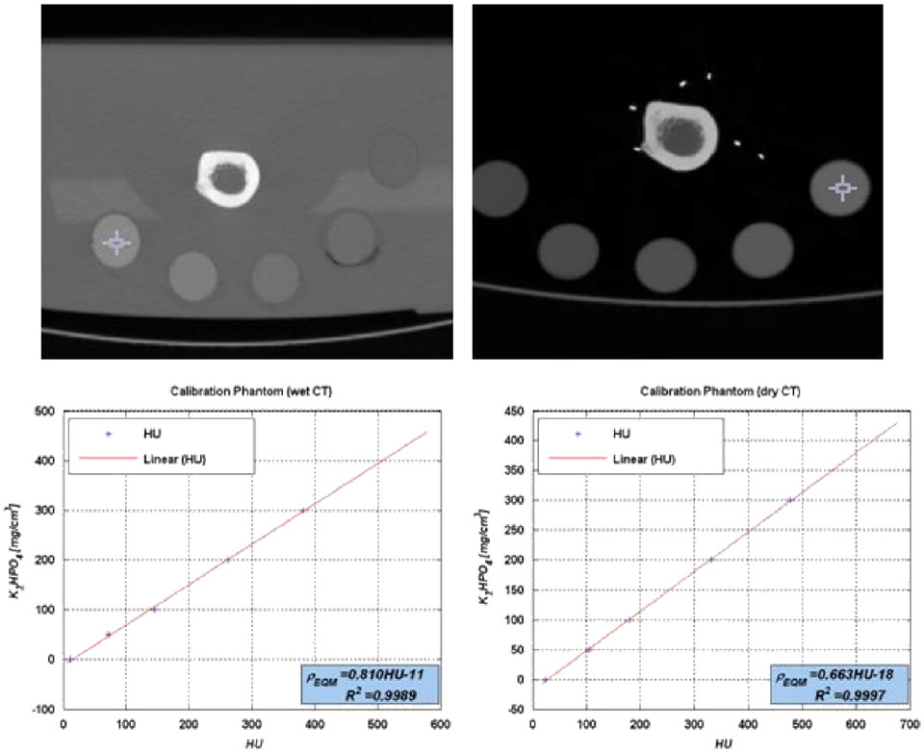

Fig. 3. ρ_{EQM} (HU) estimation. Left: CTwet scan of bone's shaft and K_2HPO_4 calibration phantoms and the linear correlation; right: CTdry scan.

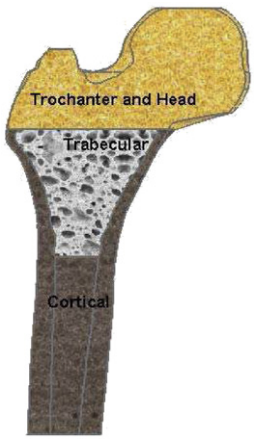

Fig. 4. Three subregions of the proximal femur, each with a different spatial function representing Young's modulus.

$E(x, y, z)$ were considered: least mean square (LMS) and WPA. The LMS algorithm was applied to approximate the discrete values of ρ_{EQM} by spatial functions using (3) or (4), providing a continuous spatial polynomial approximation. The coefficients a_{ijk} were determined so the best fit of density values in the CT scans to the function is obtained (Yosibash et al., 2007b).

$$\rho_{EQM_{wet}} = 0.81 \cdot HU - 11 \text{ [g/cm}^3\text{]}, \quad R^2 = 0.99 \tag{1}$$

$$\rho_{EQM_{dry}} = 0.663 \cdot HU - 18 \text{ [g/cm}^3\text{]}, \quad R^2 = 0.99 \tag{2}$$

$$\rho_{EQM} = \sum_{i=0}^{p_i} \sum_{j=0}^{p_j} \sum_{k=0}^{p_k} a_{ijk} x^i y^j z^k \tag{3}$$

$$\rho_{EQM} = \sum_{k=0}^{p_k} z^k \left(\sum_{i,j=0}^{p_i,p_j} a_{ijk} r^i \sin(j\theta) + \sum_{i,j=0}^{p_i,p_j} a_{ijk} r^i \cos(j\theta) \right) \tag{4}$$

Since we use E as a function of ash density (ρ_{ash}), the following relations from (Keyak and Falkinstein, 2003) are used:

$$\rho_{Ash} = 1.22 \cdot \rho_{EQM} + 0.0523 \text{ [g/cm}^3\text{]} \tag{5}$$

$$E_{Cort} = 10200 \cdot \rho_{Ash}^{2.01} \text{ [MPa]} \tag{6}$$

$$E_{Trab} = 5307 \cdot \rho_{Ash} + 469 \text{ [MPa]} \tag{7}$$

E(ρ) was defined by different formulas in each subregion (cortical and trabecular) with an assumed constant Poisson's ration of 0.3. The LMS approximation of the

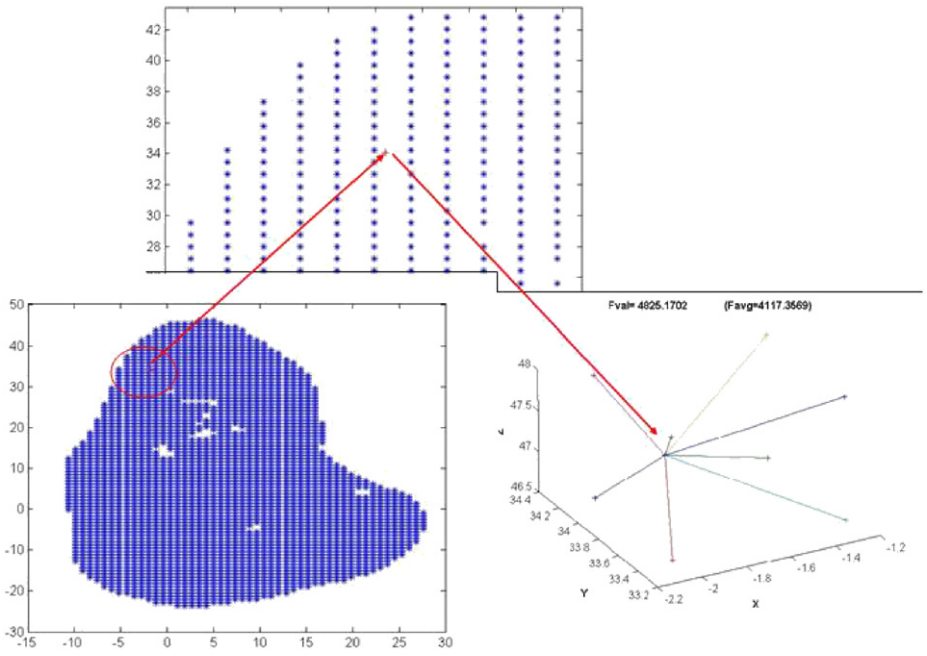

Fig. 5. Weighted point average: identifying the point in the 3D array, Gauss point value is set as the average according to its surrounding.

density is investigated as follows: in the CTwet scan several functions (3) or (4) were considered using monotonically increased polynomial degree (p_i, p_j, p_k). For each, the parameter R^2 for the LMS approximation was computed. In addition, a new method for assigning $E(x, y, z)$ to FE models directly from the CT data were used: the $E(x, y, z)$ at each integration point (Gauss points, 512 for tetrahedral elements) was extracted directly from the CT scans: CT data was converted to an array describing each pixel's location and it is equivalent to E. The value at every Gauss point is computed using a WPA method: eight vertices of a cube in which the Gauss point is located are identified (see Fig. 5) and the value at the Gauss point is computed by its relative distance from vertices. The WPA method is considered as being the most realistic but increases the computational time.

2.3. Boundary condition

Boundary conditions describe the experiments as follows: distal face was fully constrained and 1000 N load was applied on the head planar face in the proper direction (four different inclination angles). In Fig. 7 the proximal femur FE model is shown fully clamped at its lower end and loaded at 0° inclination on its head.

3. Results

3.1. FE model verification—different CT conditions

The geometrical representation and Young's modulus assignment are the main keys for constructing a FE model. The boundary detection algorithm was found to be insensitive to the wet or dry CT scans and produce almost the same geometry of the bone. Fig. 6 presents the boundary tracing results for the two different CT scans and demonstrate its accuracy at several slices. The main advantage of using ρ_{EQM} is its generality. Calibration phantoms enable same material evaluation for the wet and dry QCTs. To verify that the FE models constructed from the wet and dry QCTs yield same results we compared strains and head displacements of wetCT and dryCT models. In the FE analysis Young's modulus is represented by (3) with $p_i = p_j = p_k = 4$. Fig. 7 presents 16 points of interest (POI) used for comparison, (POI 1–13) for strain and (POI 14–16) for the displacement. POI 1–7 are located on the shaft (cortical region) and POI 8–16 on the neck and head regions. Four models describing bone different inclination angles were compared using the same 16 points. A linear regression of the wet vs. dry FE predictions for both displacements and strains is presented in Fig. 8. The linear regression demonstrates the excellent agreement between the "wet" and the "dry" models, i.e. the methods are insensitive to the media in which the bone is immersed during the CT scans.

3.2. Young's modulus assignment

Two sets of functions (Cartesian and cylindrical coordinates, Eqs. (3) and (4)) were considered for the representation of bone density in FE models. These are determined by LMS approximation using MatLab procedures. A statistical analysis is used after applying the LMS procedure to find the one that produces the highest-quality approximation for each bone region. The LMS approximation is applied to each of the three bone regions separately (cortical, trabecular, and head-troch). We denote by models A–C the FE models with different inhomogeneous Young's modulus. Model W is the one that applied the WPA method and is taken as a reference in the comparison analysis—see Table 1.

Fig. 9 presents a comparison between strain and displacement at the 16 POI using the two material representation strategies (LMS and WPA).

3.3. FE validation

To validate the CT-based FE model we compare the experimental observations (strains and displacements) to FE results. Four different models were generated based on the wet CT data, each having a different planar trimmed surface according to the experiment tilt angle. The $E(HU)$ relations (6) and (7) were used in the three different subregions and a 1000 N load was applied as traction over the entire planar face. The analyses were performed on a personal computer (Dell PWS470 Intel CPU 3.20 GHz, 3.00 GB of RAM). The average computational time for $p = 1$–4 was 22 min (for $p = 4$ was 9 min). The entire simulation process (including generation of the FE model from QCT scans and assigning material

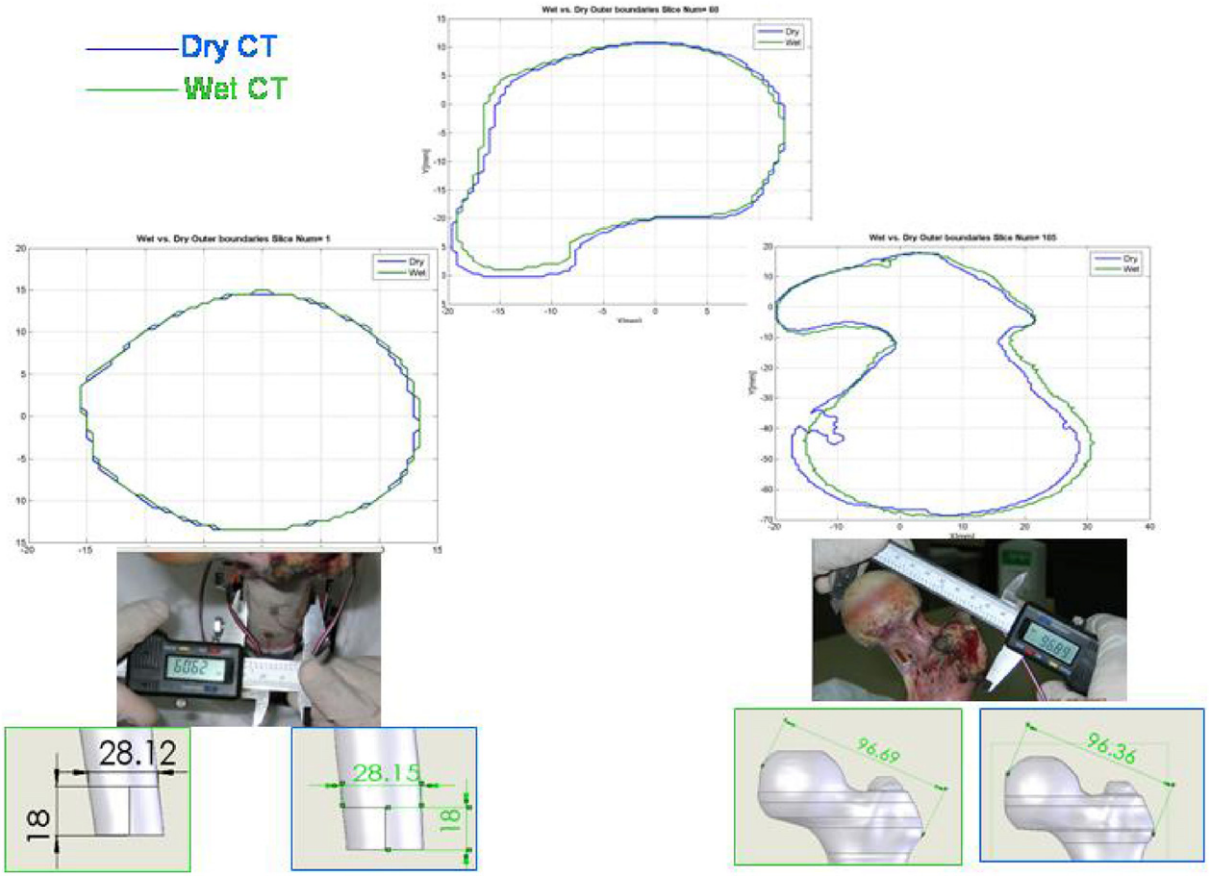

Fig. 6. Boundary tracing and geometry representation extracted from wet and dry CTs.

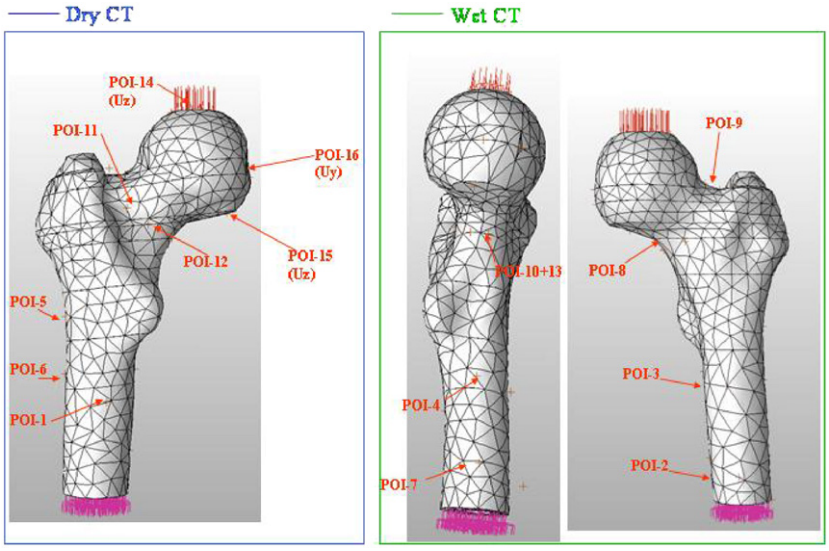

Fig. 7. FE models and 16 POI for comparison purposes.

properties) requires a couple of hours, including model verification and results inspection. All FE models show good convergence in the energy norm and in displacements and strains results for $p = 4$ or higher (see Fig. 10). The SGs and LVDTs locations were marked on the models (POI 1,3,8,10,11,12,13 for strains and 14,16 for displacements in Fig. 7), and averaged strains and displacements over the FEs face were extracted from FE results. FE strains and displacements, at various locations and for all loading conditions are summarized in Table 2. The results indicate that in most of the points the predicted strains and displacements correlate well with the experimental observations. A linear regression of experiment results vs. FE predictions, for both displacements and strains, is presented in Fig. 11. The slope of the regression line is 0.957 (very close to 1), and the linear

regression coefficient $R^2 = 0.96$ (the intercept in percentage is close to zero).

Using the two bone FE models and experiments in Yosibash et al. (2007a) together with the data presented herein we enlarge the database to further validate our method and present in Fig. 12 a linear regression of all experiments vs. the FE predictions. Three fresh frozen bones with a total of 77 experimental values recorded (61 strains and 16 displacements) were used for this validation process.

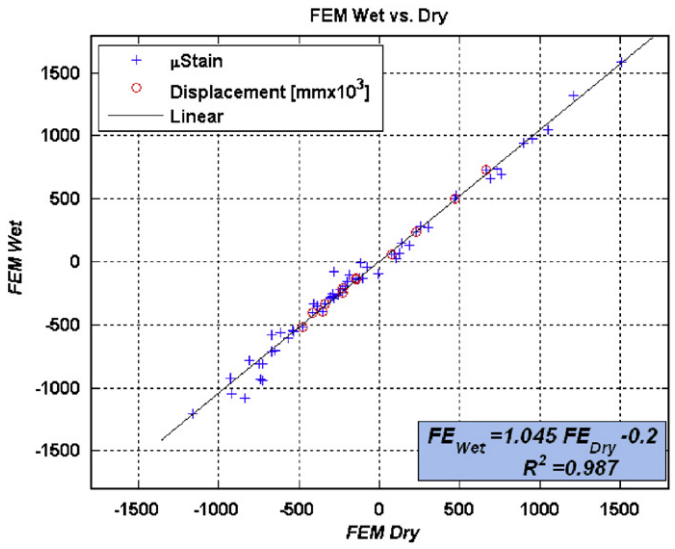

Fig. 8. Linear regression: "wet" vs. "dry" CT models. Displacements and strains for the 1000 N load of all inclination angles.

4. Discussion

This study was preformed to validate and improve the methods presented in Yosibash et al. (2007a) with the aim of generating reliable FE models of the proximal femur using subject specific QCT data. We denote by *reliable subject specific FE models* these which satisfy three conditions: (a) They were verified, i.e. the numerical errors are under control. This means that the relative error in energy norm of the overall model is guaranteed to be small and the data of interest (strains and displacements in our case) has shown to converge. (b) The FE models have been validated, i.e. the computed strains and displacements at several locations have been compared to experimental observations and show good correlation. (c) Different FE models constructed according to the same algorithm were verified and validated on a large number of experiments performed on bones harvested from donors of different ages and genders under a variety of boundary conditions.

The presented method is based on an accurate surface representation of the bone and the distinction between cortical and trabecular subregions, together with a systematic process to evaluate bone material properties. The inhomogeneous Young's modulus was represented by continuous spatial functions applied to the FE model. To further verify the reliability of the method we examined the strains and displacements prediction under

Table 1
LMS approximation: R^2 and LMS coefficient in the three bone subregions.

Model name	# of terms in expression (3) or (4) (R^2)			Cort Coeff.			Trab Coeff.			Head Coeff.		
	Cort	Trab	Head	p_i	p_j	p_k	p_i	p_j	p_k	p_i	p_j	p_k
A[a]	125 (0.94)	125 (0.94)	125 (0.79)	4	4	4	4	4	4	4	4	4
B[b]	112 (0.94)	112 (0.95)	112 (0.76)	3	3	6	3	3	6	3	3	6
C[b]	375 (0.98)	375 (0.96)	350 (0.85)	4	4	14	4	4	14	6	4	9

[a] Cartesian coordinates.
[b] Cylindrical coordinates.

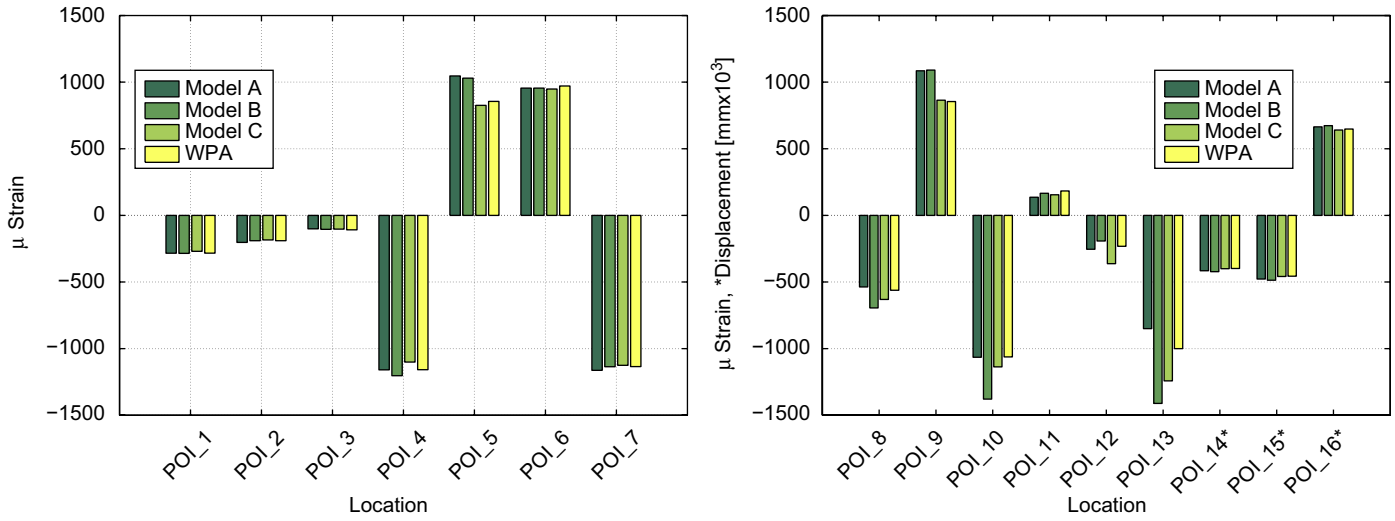

Fig. 9. FE strains and displacements obtained by two material representation strategies: LMS (models A–C) and WPA.

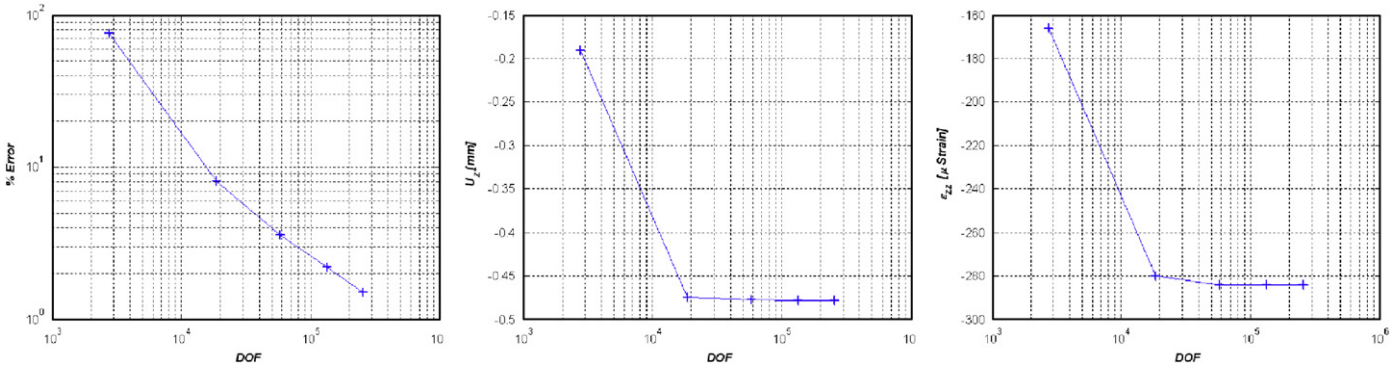

Fig. 10. Convergence in energy norm, head displacement and ε_{zz} (POI 1).

Table 2
Displacements and strains at 1000 N computed by p-FEs and experimental measurements.

Angle	POI 1 [$\mu\varepsilon$]			POI 3 [$\mu\varepsilon$]			POI 8 [$\mu\varepsilon$]		
	FEM	Exp.	Δ%	FEM	Exp.	Δ%	FEM	Exp.	Δ%
0°	−284	−328	−13	−537	−485	10	−101	−117	−13
7°	−306	−270	13	−382	−482	−21	−124	−125	−1
15°	−133	−190	−30	−528	−492	7	−200	−152	32
20°	−6	−141	−96	−568	−480	18	−241	−156	54
	POI 10 [$\mu\varepsilon$]			POI 11 [$\mu\varepsilon$]			POI 12 [$\mu\varepsilon$]		
0°	−1065	−880	21	136	209	34	−254	−299	−5
7°	−712	−776	−8	118	145	−19	−301	−306	−2
15°	−630	−750	−16	187	101	85	−293	−287	2
20°	−572	−720	−21	107	48	122	−289	−284	2
	POI 13 [$\mu\varepsilon$]			$Uz-15$ [mm × 1000]			$Uy-16$ [mm × 1000]		
0°	−850	−824	3	−478	−550	−4.5	664	560	19
7°	−716	−758	−6	−351	−400	−12	466	350	33
15°	−635	−710	−11	−229	−200	15	230	300	−23
20°	−566	−680	−17	−143	−160	−11	76	85	−11

$\Delta\% = 100(FEA - \text{Exp})/\text{Exp}$.

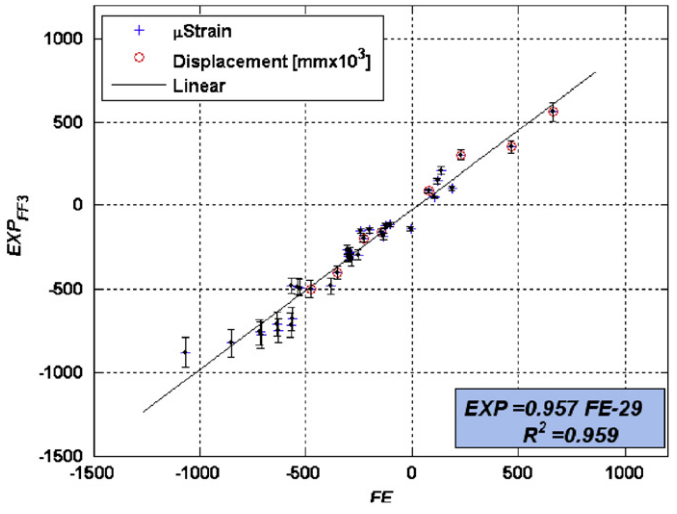

Fig. 11. Linear regression: experimental observation vs. FE displacements and strains for the 1000 N load.

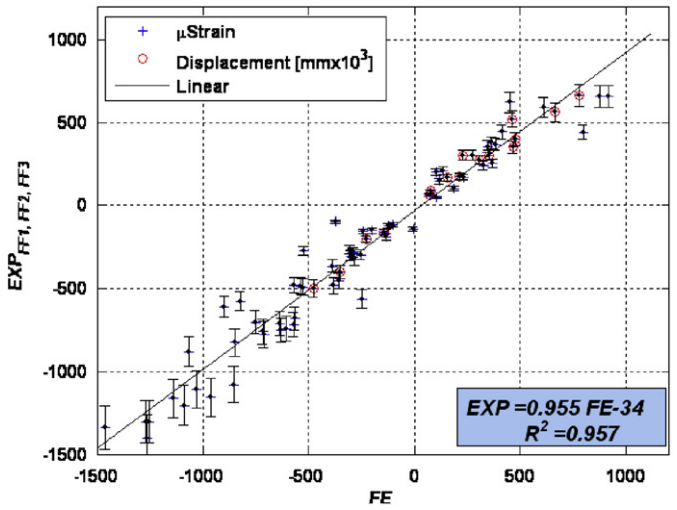

Fig. 12. Linear regression: experimental observations (fresh frozen bones 1–3) vs. FE predictions.

different CT scans conditions and used different methods for assigning inhomogeneous Young's modulus. The validation process was conducted using experimental result from three fresh frozen human femurs by comparing displacements and strains to the values extracted from the FE results.

Two key components were examined in the current study: geometry and material representation. The accuracy of CT scans-based FE models is increased when they are generated from CT scans data with the "noise" and "side" effects. The more sensitive the method is to the scan environment, the accuracy of the derived material properties and geometry decreases, and the reliability of the FE models decreases. This study has shown that the environment in which the bone is immersed during the CT scans has minor influence on the FE results using the methods presented in Yosibash et al. (2007a). The boundary detection algorithm is shown to be insensitive to CT scans environment. Calibration phantoms were used to asses bone mineral density from both CT scans, thereafter $E(\rho)$ relations were applied to evaluate Young's modulus. Although calibration phantoms cannot perfectly mimic bone attenuation coefficient, it ensures repeatability and is a methodical process to evaluate bone density, as reported in Keyak and Falkinstein (2003), Lotz et al. (1990) and Schileo et al. (2008). Using calibration phantoms, one can obtain the same density value for the same scanned object under different scanning conditions and CT machines. Considering the scanned object size and the quality of the CT scans reported in this study, the presented

method can be implement on CT scans preformed in-situ and probably even in vivo. Based on the FE result and the minor influence of the scan conditions on the FE predictions, in the authors' opinion with minor modifications this method may be used to generate reliable subject-specific FE models.

A subject-specific reliable FE model necessitates accurate evaluation of bone's material properties. This topic was further examined in the current study using two methods to represent bone inhomogeneous Young's modulus in FE models. Most studies define material properties on an element basis. In the present study, variable Young's modulus within each element was determined by two different strategies. Although the WPA method is considered as being more sensible and accurate, the comparison analysis showed excellent agreement between it and the LMS method. In a few specific locations exceptional errors (peak error of 25%) were noticed and it is probably due to the limited LMS capability of representing all bone regions with the same accuracy. The overall analysis still (average error of 4%) demonstrates that LMS is sufficiently accurate for representing variable Young's modulus in the FE model. In addition, continuous spatial functions are integrated well in the p-FEM solver and reduce numerical problems due to discrete jumps between adjacent elements. To validate our model, we used three bone experimental data as reference. The mechanical experiments were preformed on three different fresh frozen bones at several inclinations angles. The FE strains and displacements correlate well with the experimental observation with the same range of accuracy as reported in Yosibash et al. (2007a). All experimental data, strain and displacements were compared to the FE analyses ($n = 77$) together with a linear regression presented in Fig. 12. The slope of the regression line is 0.955, and the linear regression coefficient is $R^2 = 0.957$. The good agreement between the analyses and experiments are to the best of the authors' knowledge more accurate than other investigations reported in the literature.

Limitations of the present work are: (a) The FE models have been validated on three normal femurs in vitro. (b) The effect of using QCT scans data obtained in situ and in vivo still needs to be examined. (c) FE model did not take into account the known local anisotropic behavior of the bone tissue.

To conclude, a method for the construction of patient-specific p-FE models from QCT scans was investigated in this study. The method was numerically verified and validated by experimental observations. Good agreement of the analyses simulations and experiment was found comparing both displacements and strains. The errors reported in this study are reasonable for a biomechanical analysis. This study exemplifies that the presented method is in an advanced stage to be used in clinical computer-aided decision making. Investigation of the anisotropic material properties assigned to FE models of the human femur is currently underway and will be reported in future work.

Conflict of interest statement

None of the authors have any conflict of interest to declare that could bias the presented work.

Acknowledgment

The authors thank Dr. Arie Bussiba for his assistance in the experiments.

References

Bessho, M., Ohnishi, I., Matsuyama, J., Matsumoto, T., Imai, K., Nakamura, K., 2007. Prediction of strength and strain of the proximal femur by a CT-based finite element method. J. Biomechanics 40, 1745–1753.

Carter, D.R., Hayes, W.C., 1977. The compressive behavior of bone as a two-phase porous structure. J. Bone Jt. Surg. 59, 954–962.

Cody, D.D., Gross, G.J., Hou, F.J., Spencer, H.J., Goldstein, S.A., Fyhrie, D.P., 1999. Femoral strength is better predicted by finite element models than QCT and DXA. J. Biomechanics 32, 1013–1020.

Cody, D.D., Hou, F.J., Divine, G.W., Fyhrie, D.P., 2000. Short term in vivo study of proximal femoral finite element modeling. J. Ann. Biomed. Eng. 28, 408–414.

Helgason, B., Taddei, F., Palsson, H., Schileo, E., Cristofolini, L., Viceconti, M., Brynjolfsson, S., 2008. A modified method for assigning material properties to fe models of bones. Med. Eng. Phys. 30, 444–453.

Keyak, J.H., Falkinstein, Y., 2003. Comparison of in situ and in vitro CT scan-based finite element model predictions of proximal femoral fracture load. J. Med. Eng. Phys. 25, 781–787.

Keyak, J.H., Meagher, J.M., Skinner, H.B., Mote Jr., C.D., 1990. Automated three-dimensional finite element modelling of bone: a new method. J. Biomed. Eng. 12, 389–397.

Lotz, J.C., Gerhart, T.N., Hayes, W.C., 1990. Mechanical properties of trabecular bone from the proximal femur: a quantitative CT study. J. Comput. Assisted Tomography 14 (1), 107–114.

Peng, L., Bai, J., Zeng, X., Zhou, Y., 2006. Comparison of isotropic and orthotropic material property assignments on femoral finite element models under two loading conditions. J. Med. Eng. Phys. 28, 227–233.

Luo, Q., 2003. Artifacts in X-ray CT. Research Imaging Center, University of Texas Health Science Center, TX 78229. URL: ⟨http://ric.uthscsa.edu/personalpages/lancaste/DI2_Projects_2003/XrayCT_artifacts.pdf⟩.

Schileo, E., Taddei, F., Malandrino, A., Cristofolini, L., Viceconti, M., 2007. Subject-specific finite element models can accurately predict strain levels in long bones. J. Biomechanics 40, 2982–2989.

Schileo, E., Dall'Ara, E., Taddei, F., Malandrino, A., Malandrino, A., Schotkamp, T., Viceconti, M., 2008. An accurate estimation of bone density improves the accuracy of subject-specific finite element models. J. Biomechanics 41, 2483–2491.

Taddei, F., Schileo, E., Helgason, B., Cristofolini, L., Viceconti, M., 2007. The material mapping strategy influences the accuracy of CT-based finite element models of bones: an evaluation against experimental measurements. J. Med. Eng. Phys. 29, 973–979.

Wirtz, D.C., Schiffers, N., Pandorf, T., Radermacher, K., Weichert, D., Forst, R., 2000. Critical evaluation of known bone material properties to realize anisotropic FE simulation of the proximal femur. J. Biomechanics 33, 1325–1330.

Yosibash, Z., Trabelsi, N., Milgrom, C., 2007a. Reliable simulations of the human proximal femur by high-order finite element analysis validated by experimental observations. J. Biomechanics 40, 3688–3699.

Yosibash, Z., Padan, R., Joscowicz, L., Milgrom, C., 2007b. A CT-based high-order finite element analysis of the human proximal femur compared to in-vitro experiments. ASME J. Biomechanics Eng. 129 (3), 297–309.